Acta Materialia 237 (2022) 118158

Contents lists available at ScienceDirect

Acta Materialia

journal homepage: www.elsevier.com/locate/actamat

Exploration of the dislocation-electrochemistry relation in $LiFePO_4$ cathode materials

Hongjiang Chen, Sangwook Kim, Hsiao-Ying Shadow Huang*

Mechanical and Aerospace Engineering Department, North Carolina State University, R3158 Engineering Building 3, Campus Box 7910, 1840 Entrepreneur Dr., Raleigh, NC 27695 USA

ARTICLE INFO

Article history:
Received 23 April 2022
Revised 30 June 2022
Accepted 6 July 2022
Available online 14 July 2022

Keywords:
Dislocations
Cyclic voltammetry
Electrochemistry
Stress
Displacement
Lithium-ion battery

ABSTRACT

Defects, such as dislocations, in electrode materials play a significant role in the performance of lithium-ion batteries. The dislocation-electrochemistry relation has only been observed experimentally and not been fully clarified. Computational studies on this mechanism were also very limited, especially the altered cyclic voltammetry behaviors and associated effective diffusivity. This work focuses on the influences of few characteristics of dislocations on the electrochemical performance of an anisotropic cathode material, lithium iron phosphate ($LiFePO_4$). Utilizing linear elastic mechanics and the superposition principle, we study stress and displacement fields of a $LiFePO_4$ particle containing different densities and orientations of dislocations. With the mechanical-electrochemical coupling effects expressed by the modified Butler-Volmer equation and using the finite different method, the cyclic voltammetry curves for different dislocation configurations in the particle are investigated. Our results show that introducing dislocations can shift and distort the cyclic voltammetry curves, especially at one specific dislocation orientation. It is also found that the Li-ion molar fraction-dependent partial molar volume is an important prerequisite of the distortion in cyclic voltammetry curves. Moreover, the altered cyclic voltammetry curves at different scanning rates indicate the improvements of electrical power, stored electrical energy, and the effective diffusivity of lithium. Our discrete dislocation model indicates that the capacity loss of $LiFePO_4$ nanoparticles can be alleviated by introducing tailored dislocations. This study assists the understanding of electrode materials with pre-existing dislocations and provides strategies of using defect engineering to improve the kinetic performance in lithium-ion batteries.

1. Introduction

The dislocations in electrode particles have been considered as an important factor that influences the performance of lithium-ion batteries. For example, the simulation of Wei et al. [1] showed that dislocations could help spherical electrode particles avoid the formation of cracks since the tensile stress in the particles were reduced by the dislocation-induced stresses. This effect may be shown in cylindrical electrodes as well, as simulated by Li et al. [2]. In contrast to the above positive influences of dislocations in electrodes, Yan et al. [3] observed the dislocation-based crack incubation mechanism in $LiNi_{1/3}Mn_{1/3}Co_{1/3}O_2$. Moreover, Singer et al. [4] reported that dislocation networks should be the origin of the voltage fade in lithium-rich layered oxides (LRLO) $Li_{1.2}Ni_{0.133}Mn_{0.533}Co_{0.133}O_2$ during cycling because of the crystal structural changes resulted from dislocations. Thus, dislocations may have both positive and negative effects on the performance of electrodes and associated complicated dislocation-involved mechanics and electrochemistry have not been fully clarified yet.

With the development of defect engineering [5–7], controlling the dislocations in electrodes has been considered as a potential strategy to improve the performance of Li-ion batteries. For example, in the study of Yan et al. [8], the engineered edge dislocations that were generated during the fabrication of Co_3O_4 electrodes modified the surface facets of Co_3O_4 nanosheets and improved the cycling efficiency of the electrodes. It was observed that engineered dislocations have helped alleviate the volume change during cycling, supplied more nucleation sites for phase transformations, and promoted the diffusion of lithium-ions and electrons. Nevertheless, using the engineered dislocations to further optimize the electrodes of Li-ion batteries still requires a comprehensive understanding of the influences of dislocations on the particle deformation, ionic diffusion, and electrochemical reactions of electrodes.

The deformation and mechanical stress in electrode particles induced by the diffusion of lithium-ions may lead to cracks in the particles, which have been considered as an important factor for the degradation of Li-ion batteries [9–11]. Unraveling the evolu-

* Corresponding author
E-mail address: hshuang@ncsu.edu (H.-Y.S. Huang).

https://doi.org/10.1016/j.actamat.2022.118158
1359-6454/

tion of the stress field in electrodes during cycling is thus a necessary step prior utilizing dislocations to enhance the performance of Li-ion batteries. Cheng and Verbrugge [12] derived an analytical model for the diffusion-induced stress in a single spherical electrode particle providing stress evolutions for different lithiation modes. To illuminate the stress field in a more realistic electrode microstructure, Kim et al. [13] used focused ion beam and scanning electron microscopy to generate a reconstructed 3-D $LiFePO_4$ model, whose diffusion-induced Von-Mises stress was higher for a larger (dis)charging rate (C-rate). The stresses in electrodes have been shown to be coupled with lithium-ion diffusion and electrochemical reactions in several studies [14–17] and furthermore influence the kinetic performance of Li-ion batteries.

As the lifetime and performance of Li-ion batteries relate to the existing cracks and the mechanical-diffusional-electrochemical coupling effect in electrodes, the influences of dislocations on the mechanical stress fields of electrodes have been investigated in several studies: Liu et al. [18] showed the coupling effect between dislocations, diffusion, and electrochemical reactions by modeling the stresses in a spherical electrode particle. Li et al. [19] simulated the cooperative surface and dislocation effects on the diffusion-induced stress in a spherical electrode particle. Zhu et al. [20] studied the dislocation effect on the diffusion-induced stress in a hollow spherical particle, in which the influence of the wall thickness of the hollow particle on the dislocation effect was discussed. Among above contributions, dislocations were demonstrated to suppress the fractures in electrodes since the tensile stress in the particles could be reduced by the presence of dislocations.

Most of the studies modeling the dislocation-involved stress fields in electrode particles were based on the assumption of isotropic materials while also neglecting the effect of the orientations of dislocations, which is over-simplified for an anisotropic material such as Li_YFePO_4, where Y indicates the fraction of Li ions [21]. That is, material properties of Li_YFePO4 varies during (de)lithiation due to molar fraction changes of lithium [21,22]. Huang and Wang [23] had first incorporated a model from Indenbom and Lothe [24] to elucidate the mechanical effects of the dislocation orientation in a Li_YFePO_4 particle. Furthermore, Dhiman and Huang [25] studied the influences of phase separation induced by the lithium molar fraction variations and different dislocation orientations on cyclic voltammetry (CV) behaviors for a Li_YFePO_4 particle. Specifically, the stress field were studied while incorporating the electrochemical reaction by using the modified Butler Volmer equation [25,26].

In addition, dislocations can appear not only due to the fabrication of electrodes but also during the (dis)charging cycling. The state of charge (SOC) of an electrode particle is an important factor generating an array of dislocations in a particle during (de)lithiation. For example, in a thin film anode, lithiation speed and the diffusion layer thickness, which represent the SOC, highly impacted the nucleation and density distribution of the misfit dislocations in the anode, as reported by Li et al. [27]. Ulvestad et al. [28] observed that the dislocation lines in a nano-sized $LiNi_{0.5}Mn_{1.5}O_4$ cathode particle moved towards the boundary of the particle, in which the positions of the dislocation lines depended on the SOC of the particle. Nevertheless, the relation between the dislocation density and the SOC is electrode material dependent. Singer et al. [4] reported that the dislocation density of the LRLO particles is much more sensitive to electrical potential (i.e., an indicator of the SOC), compared to the $LiNi_{0.8}Co_{0.15}Al_{0.05}O_2$ (NCA) particle. Moreover, the correlation of the dislocation density to the electrical potential for the LRLO particles is observed to be related to the geometries of the particles [4]. Aforementioned studies suggest that these characteristics of dislocations have substantial effects on the electrochemical performance, which has not yet been investigated for Li_YFePO_4. Due to the anisotropy of Li_YFePO_4, it is arguable that the dislocation density should have a strong influence on the dislocation orientation, and vice versa.

To further understand the effects of dislocations on the anisotropic electrodes with phase transformations such as Li_YFePO_4, this study focuses on the influences of the dislocation density and orientation, the associated effective diffusivities of a Li_YFePO_4 particle, as well as the related electrochemical performance of Li_YFePO_4. Based on linear elastic mechanics, the superposition principle, and the mechanical-electrochemical coupling effect, the stress fields, displacement fields, and CV curves at different scan rates are studied and discussed. The coupling effect between mechanics and electrochemistry is an intrinsic property of electrode materials, which has been shown in many articles [14,29–32]. In the current study, we explore the coupling effect to further investigate benefits of engineered dislocations and the potential to enhance the electrode performance of Li-ion batteries.

2. Methods

2.1. Mechanics of dislocations for Li_YFePO_4 cathode particles

The stress field resulted from a dislocation in a anisotropic material Li_YFePO_4 particle is calculated using Eq. (1) [24] as shown below,

$$\sigma_{ij} = \frac{b_x\lambda\left(C_{12}-\bar{C}_{11}\right)}{4\pi q^2\tau^2\bar{C}_{11}C_{66}\sin\phi}\begin{Bmatrix} C_{ij11}\left[\left(\bar{C}_{11}+C_{12}+C_{66}\right)r_x^2r_y+\lambda^2C_{66}r_y^3\right] \\ -C_{ij12}\left(\bar{C}_{11}+C_{12}\right)\left(r_x^3-\lambda^2r_xr_y^2\right) \\ -\frac{C_{ij22}}{\bar{C}_{22}}\left[\left(C_{12}^2+\bar{C}_{11}C_{12}+2C_{12}C_{66}+\bar{C}_{11}C_{66}\right)r_x^2r_y-\bar{C}_{11}C_{66}\lambda^2r_y^3\right] \end{Bmatrix} , \\ -\frac{b_y\lambda\left(C_{12}-\bar{C}_{11}\right)}{4\pi q^2\tau^2\bar{C}_{11}C_{66}\sin\phi}\begin{Bmatrix} C_{ij22}\left[\left(\bar{C}_{11}+C_{12}+C_{66}\right)\lambda^2r_xr_y^2+C_{66}r_x^3\right] \\ -C_{ij12}\left(\bar{C}_{11}+C_{12}\right)\left(\lambda^2r_y^3-r_x^2r_y\right) \\ -\frac{C_{ij11}}{\bar{C}_{11}}\left[\left(C_{12}^2+\bar{C}_{11}C_{12}+2C_{12}C_{66}+\bar{C}_{11}C_{66}\right)\lambda^2r_xr_y^2-\bar{C}_{11}C_{66}r_x^3\right] \end{Bmatrix} \tag{1}$$

with $\bar{C}_{11}=(C_{11}C_{22})^{1/2}$, $\lambda=(C_{11}/C_{22})^{1/4}$, $\phi=\frac{1}{2}\cos^{-1}\left(\frac{C_{12}^2+2C_{12}C_{66}-\bar{C}_{11}^2}{2\bar{C}_{11}C_{66}}\right)$, $q^2=r_x^2+2r_xr_y\lambda\cos\phi+r_y^2\lambda^2$, and $\tau^2=r_x^2-2r_xr_y\lambda\cos\phi+r_y^2\lambda^2$, where σ_{ij} is the stress component of the particle, (b_x, b_y) is the Burgers vector of the dislocation, C_{ij} and C_{mnpq} are the engineering component and the theoretical component of the stiffness tensor of the particle, respectively, (r_x, r_y) is the radius vector in the particle with respect to the dislocation core.

The displacement field resulted from a dislocation in a anisotropic material Li_YFePO_4 particle is calculated using Eqs. (2) and (3) [24] as shown below,

$$u_x = \frac{b_x}{4\pi}\left[\omega+\frac{\bar{C}_{11}^2-C_{12}^2}{2\bar{C}_{11}C_{66}\sin2\phi}\ln\left(\frac{q}{\tau}\right)\right]+\frac{b_y}{4\pi\lambda\bar{C}_{11}\sin2\phi} \left[\left(\bar{C}_{11}-C_{12}\right)\cos\phi\ln\left(q\tau\right)-\left(\bar{C}_{11}+C_{12}\right)\eta_x\sin\phi\right], \tag{2}$$

$$u_y = -\frac{\lambda b_x}{4\pi\bar{C}_{11}\sin2\phi}\left[\left(\bar{C}_{11}-C_{12}\right)\cos\phi\ln\left(q\tau\right)-\left(\bar{C}_{11}+C_{12}\right)\eta_y\sin\phi\right] +\frac{b_y}{4\pi}\left[\omega-\frac{\bar{C}_{11}^2-C_{12}^2}{2\bar{C}_{11}C_{66}\sin2\phi}\ln\left(\frac{q}{\tau}\right)\right], \tag{3}$$

where u_x and u_y are the horizontal and the vertical components of the displacement, respectively. ω, η_x, and η_y are named auxiliary angles.

During lithiation and delithiation, a Li_YFePO_4 cathode particle has three stages: Li-poor phase, Li-rich phase, and two-phase coexistence [22]. Both Li-poor and Li-rich phases have the orthorhombic crystal structure [33], which satisfies the symmetry prerequisite of Eqs. (1)–(3) [24]. The material properties (i.e., stiffness coefficients) of the particle at each stage during (de)lithiation are different [21]. In the two-phase coexistence region, we assume that the overall stiffness of the particle is a linear function (i.e., rule of mixture) of the phase fraction of the Li-rich phase: $C_{ij} = (1 - x_p)C_{(FePO_4)ij} + x_pC_{(LiFePO_4)ij}$, where x_p is the Li-rich phase fraction, $x_p = 0$ indicates the single Li-poor phase, $x_p = 1$ indicates the single Li-rich phase, $C_{(FePO_4)ij}$ is the stiffness component of the Li-poor phase, and $C_{(LiFePO_4)ij}$ is the stiffness component of the Li-rich phase [34–36]. Since this study emphasizes the influence of dislocation-induced stress on electrochemical performance, the material properties (i.e., stiffness and partial molar volume) of Li_YFePO_4 are assumed to be independent of dislocations for simplicity.

The auxiliary angles ω, η_x, and η_y in Eqs. (2) and (3) are obtained by numerically solving the equations below,

$$[D_\Psi] \cdot \omega = \frac{2\sec^2(\Psi)\sin(\phi)\left[\lambda + \lambda^3\tan^2(\Psi)\right]}{1 - 2\lambda^2\cos(2\phi)\tan^2\Psi + \lambda^4\tan^4\Psi}, \tag{4}$$

$$[D_\Psi] \cdot \eta_x = -\frac{2\lambda^2\sec^2(\Psi)\sin(2\phi)\tan\Psi}{1 - 2\lambda^2\cos(2\phi)\tan^2\Psi + \lambda^4\tan^4\Psi}, \tag{5}$$

$$[D_\Psi] \cdot \eta_y = \frac{2\lambda^2\csc^2(\Psi)\sin(2\phi)\cot\Psi}{\lambda^4 - 2\lambda^2\cos(2\phi)\cot^2\Psi + \cot^4\Psi}, \tag{6}$$

with the boundary conditions $\omega(\Psi = 0) = 0$, $\eta_x(\Psi = 0) = 0$, and $\eta_y(\Psi = 0) = 0$, where Ψ is the azimuth relative to the Burgers vector, with the range $-\pi < \Psi \leq \pi$, and $[D_\Psi]$ is the finite difference matrix with respect to Ψ. The derivation of Eqs. (4)–(6) are shown in the **Appendix**.

We use the superposition principle to calculate the stress and displacement fields induced by multiple dislocations in a Li_YFePO_4 particle: the overall stress and displacement of a particle are the summations of the stress and displacement resulted from each dislocation calculated using Eqs. (1)–(3). For simplicity, we use a 2-D particle model with the plane strain condition to investigate the stress and displacement fields resulted from dislocations. The geometry of the particle model in this study is adapted from Dhiman and Huang [25], which is a rectangle of 100 nm × 60 nm, containing 60 unit cells. The size of the region dominated by the nonlinear deformation around a dislocation core is about 4 nm × 4 nm [37], which is small enough compared to the size of the particle model. As the nonlinear effect is negligible, Eqs. (1)–(3) are valid for the particle size 100 nm × 60 nm. We define the center of the rectangle as the origin of the Cartesian coordinate frame, in which the coordinate ranges of the particle are [-50 nm, 50 nm] for the x-axis and [-30 nm, 30 nm] for the y-axis. We assumed that the length of a dislocation line in our particle model is 90% of the particle thickness along the z direction, hence the dislocation density for one dislocation is 1.5×10^{10} cm^{-2}, which agrees with the measurement in Singer et al. [4].

To investigate the influences of the density and orientation of dislocations, we assign five dislocations at different locations: dislocation#1 at (-20 nm, -12 nm) with three different Burgers vector directions discussed below, dislocation#2 at (40 nm, 24 nm) with the Burgers vector (1, 0), dislocation#3 at (25 nm, -15 nm) with the Burgers vector (-1, 0), dislocation#4 at (-40 nm, 17 nm) with the Burgers vector (1, 0), and dislocation#5 at (0, -24 nm) with the Burgers vector (-1, 0). Three Burgers vector directions at dislocation#1 are chosen from the set {(1, 0), (0, -0.6), (-1, 0)}, where (1, 0) is named orientation-1, (0, -0.6) denotes orientation-2, and (-1, 0) represents orientation-3. Five dislocations compose four groups with different dislocation densities for simulations: group A contains two dislocations (i.e., dislocation#1 and dislocation#2), group B contains three dislocations (i.e., dislocation#1, dislocation#2, and dislocation#3), group C contains four dislocations (i.e., dislocation#1, 2, 3, and 4), group D contains five dislocations (i.e., dislocation#1, 2, 3, 4, and 5), where each group includes three different orientations of dislocation#1 (i.e., (1, 0), (0, -0.6), or (-1, 0)).

2.2. Kinetics of CV scan for Li_YFePO_4 cathode particles

During the CV scan of a Li_YFePO_4 cathode material, the difference between the instant electrical potential of the particle and the equilibrium electrical potential of two-phase coexistence is named "overpotential" and denoted by $\Delta\varphi$, whose range is -0.3 V < $\Delta\varphi$ < 0.3 V in this study. In a complete scan cycle, $\Delta\varphi$ changes from 0.3 V to -0.3 V with a scan rate ν, and then increases back to 0.3 V with the same ν. To present the detailed influences of dislocations on the kinetic performance of Li_YFePO_4 materials, we simulate 5 different scan rates: 1mV/s, 2mV/s, 4mV/s, 8mV/s, and 16mV/s. Collectively, a total of 61 simulations are conducted, including the case of perfect crystals with no dislocations.

As mentioned in Tang et al. [38], the required activation energy for the phase transformation from Li-rich phase to Li-poor phase decreases with increased $\Delta\varphi$, and eventually reaches zero at the critical overpotential $\Delta\varphi_c$. In this regard, a Li_YFePO_4 particle would spontaneously exhibit the single Li-poor phase when $\Delta\varphi \geq \Delta\varphi_c$. During the quasi-equilibrium process, $\Delta\varphi_c$ has the lowest value $\Delta\varphi_c^*$= 30.283 mV [38]. As CV scans are non-equilibrium processes, the required $\Delta\varphi_c$ for CV scans should be higher than $\Delta\varphi_c^*$ due to electrochemical polarization [39]. Although the electrochemical polarization should be different for different electric currents, the required overpotential of Li_YFePO_4 for generating Faradic current may show little variations in the CV scans at different scan rates, which is around 60 mV for scan rates from 0.5 mV/s to 15 mV/s [40,41]. The total $\Delta\varphi_c$ hence should be around 90mV for different scan rates. For the sake of simplicity, we select that $\Delta\varphi_c = 3\Delta\varphi_c^*$ in our simulation of CV scans with all five scan rates mentioned above (i.e., 1 mV/s, 2 mV/s, 4 mV/s, 8 mV/s, and 16 mV/s). In addition, the critical overpotential of the phase transformation should have two values: a higher value and a lower one to present two boundaries at the two-phase coexistence region. The higher value $\Delta\varphi_c$ is the lowest overpotential for the Li-poor single phase ($x_p = 0$), and the lower value is the highest overpotential for the Li-rich single phase ($x_p = 1$). The lower value indicates the critical point of zero activation energy for the phase transformation from Li-poor phase to Li-rich phase. For simplicity, it is acceptable to assume that the transformation from Li-poor phase to Li-rich phase is symmetric to the transformation from Li-rich phase to Li-poor phase, which indicates that the overpotential region of the single Li-rich phase is $\Delta\varphi \leq -\Delta\varphi_c$. Thus, the phase fraction x_p may be considered as a piecewise function of $\Delta\varphi$ as follows: $x_p = 0$ for $\Delta\varphi \geq \Delta\varphi_c$; $0 < x_p < 1$ for $-\Delta\varphi_c < \Delta\varphi < \Delta\varphi_c$; and $x_p = 1$ for $\Delta\varphi \leq -\Delta\varphi_c$, where x_p is assumed to be a linear function of $\Delta\varphi$ in the two-phase coexistence region ($0 < x_p < 1$). The stiffness coefficients of the particle during the two-phase coexistence depend on the phase fraction x_p when $\Delta\varphi$ decrease from 90.849 mV to -90.849 mV.

As the process of the phase transformation during CV scans has been explicitly elucidated, we may use Fickian diffusion to simplify kinetics of the Li_YFePO_4 particle, which are shown in Eqs. (7) and (8) below:

$$\frac{\partial c}{\partial t} = D\nabla^2 c, \tag{7}$$

where c is the concentration of oxidized or reduced species, D is the bulk diffusivity, ∇^2 is the Laplacian operator, and t is time. To solve Eq. (7), we need one initial condition and two boundary conditions. The initial condition is $c_O(t=0) = c_O^*$ with $c_R(t=0) = 0$, where c_O is the concentration of the oxidized species, c_O^* is the maximum concentration of the oxidized species, c_R is the concentration of the reduced species. We use the semi-infinite boundary condition as the 1st boundary condition of Eq. (7) since the thickness of the diffusion layer during CV scans is assumed to be very small relative to the size of the whole particle. The 2nd boundary condition is given by Eq. (8) below,

$$\frac{i}{F} = -D\nabla c_R, \tag{8}$$

where i is the electric current density on the particle surface and F is the Faraday's constant.

The current density of a Li_YFePO_4 particle is controlled by chemical kinetics on the particle surface, which involves the mechanical stress resulted from dislocations and the electrical potential of the particle. We adopt the modified Butler-Volmer equation [25] shown below for the current density i in Eq. (8):

$$i = i_0\left\{\frac{c_O(0,t)}{c_O^*}\exp\left(-\alpha\frac{F\Delta\varphi - \sigma_{hAVG}\Omega}{RT}\right) - \frac{c_R(0,t)}{c_R^*}\exp\left[(1-\alpha)\frac{F\Delta\varphi - \sigma_{hAVG}\Omega}{RT}\right]\right\}, \tag{9}$$

with $i_0 = -Fk_0$, where i_0 is the exchange current density, k_0 is the reference pre-exponential factor, $c_O(0,t)$ is the concentration of the oxidized species on the particle surface, $c_R(0,t)$ is the concentration of the reduced species on the particle surface, c_R^* is the maximum concentration of the reduced species, α is the symmetry factor in chemical kinetics, σ_{hAVG} is the average hydrostatic stress of the particle, R is the gas constant, T is temperature, and Ω is the partial molar volume of Li in the particle, which is assumed to be a linear function of the molar fraction of occupied Li sites as shown below,

$$\Omega = \Omega_{AVG}\left[2k\left(y_{Li} - \frac{1}{2}\right) + 1\right], \tag{10}$$

where Ω_{AVG} is the average partial molar volume of Li, k is a material property (i.e., fraction coefficient), and y_{Li} is the molar fraction of occupied Li sites. In the modified Butler-Volmer equation (Eq. (9)), Ω is calculated using the value of y_{Li} on the particle surface governed by Eqs. (7) and (8), σ_{hAVG} is the mean of the hydrostatic stress σ_h over the 2-D particle model, with $\sigma_h = \frac{1}{3}(\sigma_{xx} + \sigma_{yy} + \sigma_{zz})$, where σ_{xx}, σ_{yy}, and σ_{zz} are stress components calculated using Eq. (1), with x, y, and z corresponding to the indices 1, 2, and 3, respectively.

The kinetic performance of a Li_YFePO_4 particle can be revealed by a single variable, named effective diffusivity, which represents the combined performance of the Li diffusion in the particle and the electrochemical reaction on the particle surface. We use the Randles-Sevcik equation [42] shown below to calculate the effective diffusivity of the particle containing different dislocation groups:

$$i_p = 0.4463Fc_O^*\left(\frac{F\nu D_{RS}}{RT}\right)^{\frac{1}{2}}, \tag{11}$$

where i_p is the peak current density and D_{RS} is the effective diffusivity.

2.3. Algorithm and parameters

The simulation algorithm coded with MATLAB includes nine steps as follows: (1) We solve Eqs. (4)–(6) to obtain the numerical auxiliary angle functions $\omega(\Psi)$, $\eta_x(\Psi)$, and $\eta_y(\Psi)$. (2) After discretizing the 2-D particle model, the stress components of all grid nodes are calculated using Eq. (1) for each dislocation. (3) We calculate the angles between the radius vectors of all grid nodes and the Burgers vectors of dislocations, and then calculate the auxiliary angles of all grid nodes using the interpolation method with the numerical functions $\omega(\Psi)$, $\eta_x(\Psi)$, and $\eta_y(\Psi)$. (4) For each dislocation, the displacement components of all grid nodes are obtained by substituting the auxiliary angles from step (3) into Eqs. (2) and (3). (5) We sum the stresses and displacements induced by all dislocations in the particle model. (6) By repeating steps (2) to (5), the average hydrostatic stresses at different phase fractions are calculated for all dislocation groups. (7) We calculate the numerical relations between σ_{hAVG} and $\Delta\varphi$ for all dislocation groups using the interpolation method with the relation between x_p and $\Delta\varphi$ mentioned in Section 2.2. (8) Based on the numerical functions $\sigma_{hAVG}(\Delta\varphi)$, we use the finite difference method shown in Bard and Faulkner [43] to solve Eqs. (7)–(10), and then obtain the electric current densities for all scan rates and all dislocation groups. (9) We substitute the peak current densities from step (8) into the Randles-Sevcik equation (Eq. (11)) to solve the effective diffusivities D_{RS} for all dislocation groups.

In Eqs. (1)–(3), the strategy of adapting phase fraction-dependent anisotropic materials of $LiFePO_4$ are obtained from Kim and Huang [34] and ChiuHuang and Huang [35,36]. Other parameters used for the simulation are listed in Table 1. For different distribution of dislocations at different scan rates, the ranges of Li fraction for two-phase coexistence during scans should be different. It is necessary to assign the range of Li fraction for one case of simulation to fit the material parameters in the modified Butler-Volmer equation and the partial molar volume of Li in the particle (i.e., Eqs. (9) and (10)). According to the open-circuit voltage of Li_YFePO_4 shown in Yamada et al. [44], the range of the molar fraction of occupied Li sites for two-phase coexistence during the quasi-equilibrium process is $0.05 < y_{Li} < 0.89$. That is, Li-ion molar fraction $y_{Li} = 0.05$ when phase fraction $x_p = 0$, and Li-ion molar fraction $y_{Li} = 0.89$ when phase fraction $x_P = 1$. We select this range and the dislocations of group D/orientation-3 (-1, 0) with $\nu = 0.65$ mV/s as the conditions of fitting the material parameters k_0 in the modified Butler-Volmer equation (Eq. (9)), Ω_{AVG} and k in the equation of partial molar volume of Li (Eq. (10)).

Table 1
Material parameters used for the simulation. #Estimated value based on the results in Maxisch and Ceder [21]. ‡Estimated value based on the results in Churikov et al. [48]. †Estimated value fit to the results in Yamada et al. [44].

Parameter	Unit	Value	Parameter	Unit	Value
c_O^*	mol/m^3	1×10^{6} #	k_0	$mol\cdot m^{-2}\cdot s^{-1}$	1×10^{-8} †
c_R^*	mol/m^3	1×10^{6} #	T	K	298.15
D	m^2/s	1×10^{-17} ‡	k	-	0.848 †
α	-	0.5	Ω_{AVG}	m^3/mol	1.5×10^{-5} †

3. Results and discussion

Fig. 1 displays the stress and displacement fields of the Li_YFePO_4 particle model with different dislocation densities, where dislocation#1 with orientation-1 (1, 0) and the phase fraction$x_p = 0.9$ of the particle. The group A includes dislocation#1 and dislocation#2. The group B contains dislocation#1, 2, and 3. The group C has dislocation#1, 2, 3, and 4. The group D includes all five dislocations. The Burgers vectors of dislocation#1, 2, 3, 4, and 5 in Fig. 1 are (1, 0), (1, 0), (-1, 0), (1, 0), and (-1, 0), respectively. As the directions of the Burgers vectors of all dislocations are (1, 0) or (-1, 0), only u_x shows the sharp interfaces which presents the location of slip planes of dislocations. Fig. 2 shows the stress and

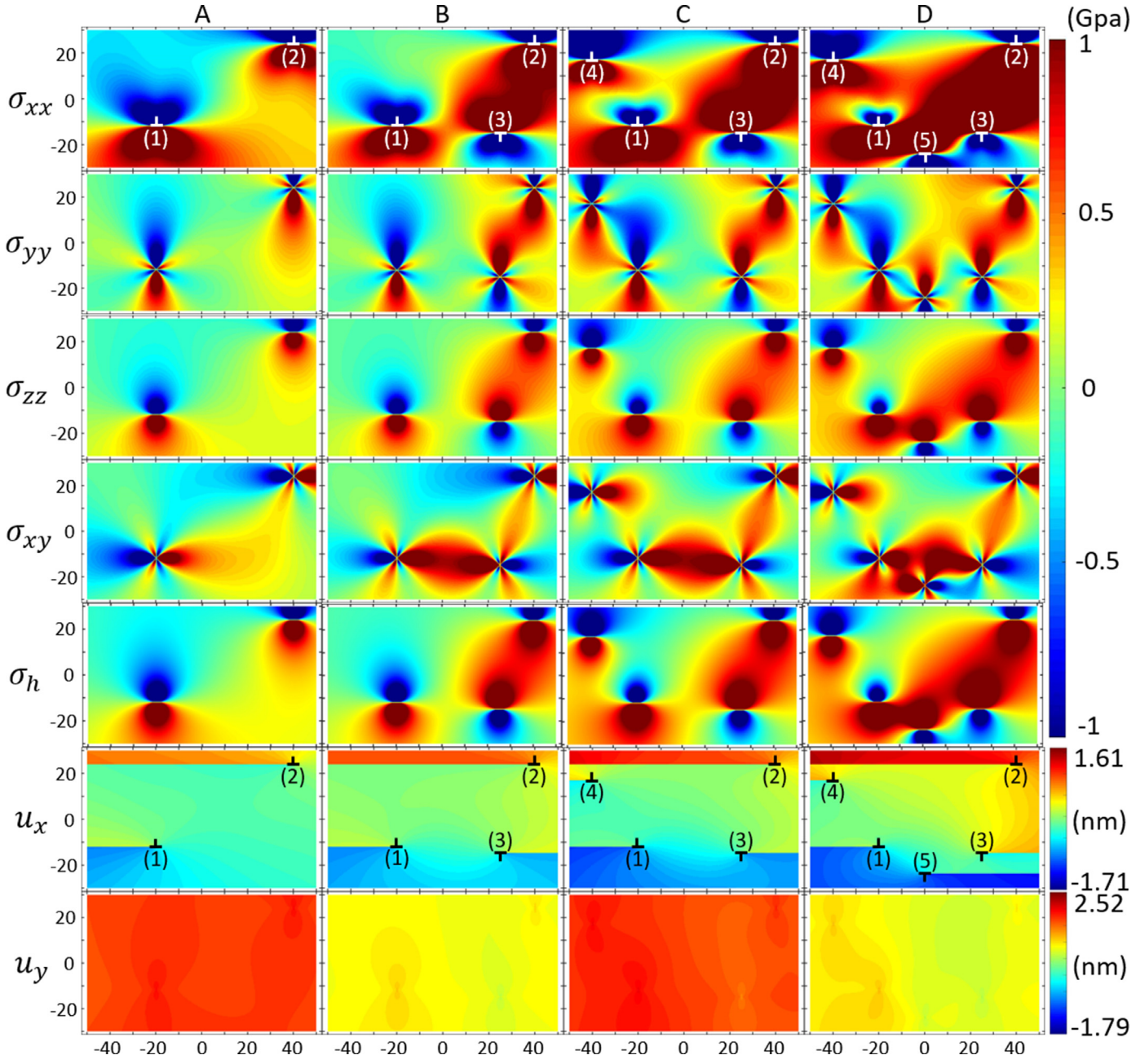

Fig. 1. Stress fields and displacement fields of a Li_YFePO_4 particle for different dislocation densities when dislocation#1 with orientation-1 and phase fraction $x_p = 0.9$. Group A has dislocation#1 and 2. Group B has dislocation#1, 2, and 3. Group C has dislocation#1, 2, 3, and 4. Group D has dislocation#1, 2, 3, 4, and 5. The Burgers vectors of dislocation#1, 2, 3, 4, and 5 are (1, 0), (1, 0), (-1, 0), (1, 0), and (-1, 0), respectively. With a higher dislocation density, the larger average value of hydrostatic stress $\sigma_h = (\sigma_{xx} + \sigma_{yy} + \sigma_{zz})/3$ suggests a higher electrical potential of the particle. The sharp interfaces in displacement fields indicate where the slip planes of dislocations locate.

displacement fields when the Burgers vector of dislocation#1 is (0, -0.6) (orientation-2). The phase fraction and the arrangements of dislocation#2, 3, 4, 5 in Fig. 2 are the same as those in Fig. 1, for easy comparison to demonstrate the effects of dislocation orientation. The slip plane of dislocation#1 with orientation-2 (0, -0.6) is presented by the corresponding sharp interface of u_y in Fig. 2. The stress and displacement fields of the particle for orientation-3 (-1, 0) of dislocation#1 are shown in Fig. 3, in which the phase fraction and the arrangements of dislocation#2, 3, 4, 5 are the same as those in Figs. 1 and 2. The sharp interface of u_x around dislocation#1 in Fig. 3 indicates the slip plane of dislocation#1 with orientation-3 (-1, 0).

In Figs. 1–3, from group A to group D, the average values of σ_{xx}, σ_{yy}, and σ_{zz} increase for all orientations of dislocation#1, which indicates a larger average hydrostatic stress for a higher dislocation density. Hence, using the modified Butler-Volmer equation (Eq. (9)) yields that increasing the dislocation density may enhance the electrical potential of Li_YFePO_4 cathodes. The sharp interfaces (i.e., lattice slip planes) in displacement fields in Figs. 1–3 reveal the dislocation-induced plastic deformation of the particle, where the existence of lattice slip plane is the key indicator of discrete plastic deformation at the interface. Of note, the total plastic strain of a crystal particle can be the accumulation of discrete dislocation plasticity from multiple dislocations. With the increased dislocation density, differences between the maximum and minimum displacement fields are observed, indicating enlarged average plastic strains for all orientations of dislocation#1 (Figs. 1–3).

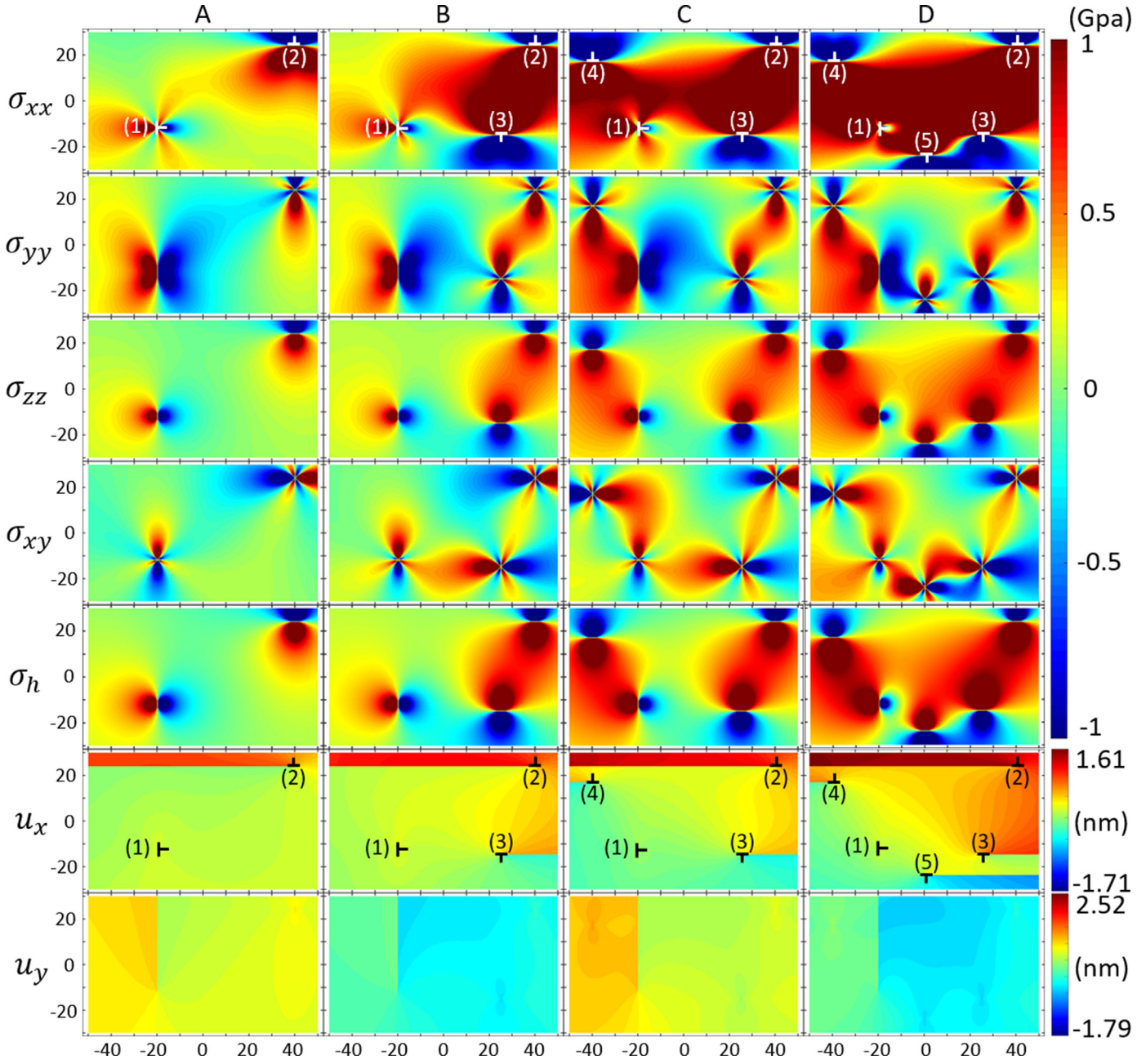

Fig. 2. Stress fields and displacement fields of a Li_YFePO_4 particle for different dislocation densities when dislocation#1 with orientation-2 and phase fraction $x_p = 0.9$. Group A has dislocation#1 and 2. Group B has dislocation#1, 2, and 3. Group C has dislocation#1, 2, 3, and 4. Group D has dislocation#1, 2, 3, 4, and 5. The Burgers vectors of dislocation#1, 2, 3, 4, and 5 are (0, -0.6), (1, 0), (-1, 0), (1, 0), and (-1, 0), respectively. With a higher dislocation density, the larger average value of hydrostatic stress $\sigma_h = (\sigma_{xx} + \sigma_{yy} + \sigma_{zz})/3$ suggests a higher electrical potential of the particle. The sharp interfaces in displacement fields indicate where the slip planes of dislocations locate.

By comparing Figs. 1–3, we observe the effect of different dislocation slip directions, i.e., the dislocation orientation, on stress fields. As shown in Eq. (1), the stress induced by each dislocation core is influenced by the dislocation orientation. The average stress of a particle is hence different for different dislocation orientations. For each dislocation density, the orientation-3 (-1, 0) (Fig. 3) exhibits the highest average values of σ_{xx}, σ_{yy}, σ_{zz}, and hydrostatic stress σ_h of the particle. Based on the modified Butler-Volmer equation (Eq. (9)), we thus deduce that the particle with orientation-3 (-1, 0) for dislocation#1 exhibits the highest electrical potential in CV scans.

The detailed influence of the dislocation orientation on the electrochemical performance of the Li_YFePO_4 particle model is revealed by CV curves for different dislocation densities in Fig. 4, where the scan rate of each CV curve is 16 mV/s. In the gray region (-90.849 mV $< \Delta\varphi <$ 90.849 mV) in Fig. 4, the Li_YFePO_4 particle shows two-phase coexistence. The stiffness coefficients of the particle during two-phase coexistence depend on the phase fraction x_p that is assumed to change linearly from 0 to 1 when $\Delta\varphi$ decrease from 90.849 mV to -90.849 mV. For every orientation of dislocation#1, the CV curve with a higher dislocation density shows a larger shift and stronger distortion relative to the CV curve with no dislocation. This comparison indicates that the dislocation density may help Li_YFePO_4 provide larger electrical power, suggesting better kinetic performance. By comparing Fig. 4**a-c**, we observe the extents of the dislocation-induced shift and distortion of a CV curve relate to the dislocation orientation. For every dislocation density, the CV curve with orientation-3 (-1, 0) for disloca-

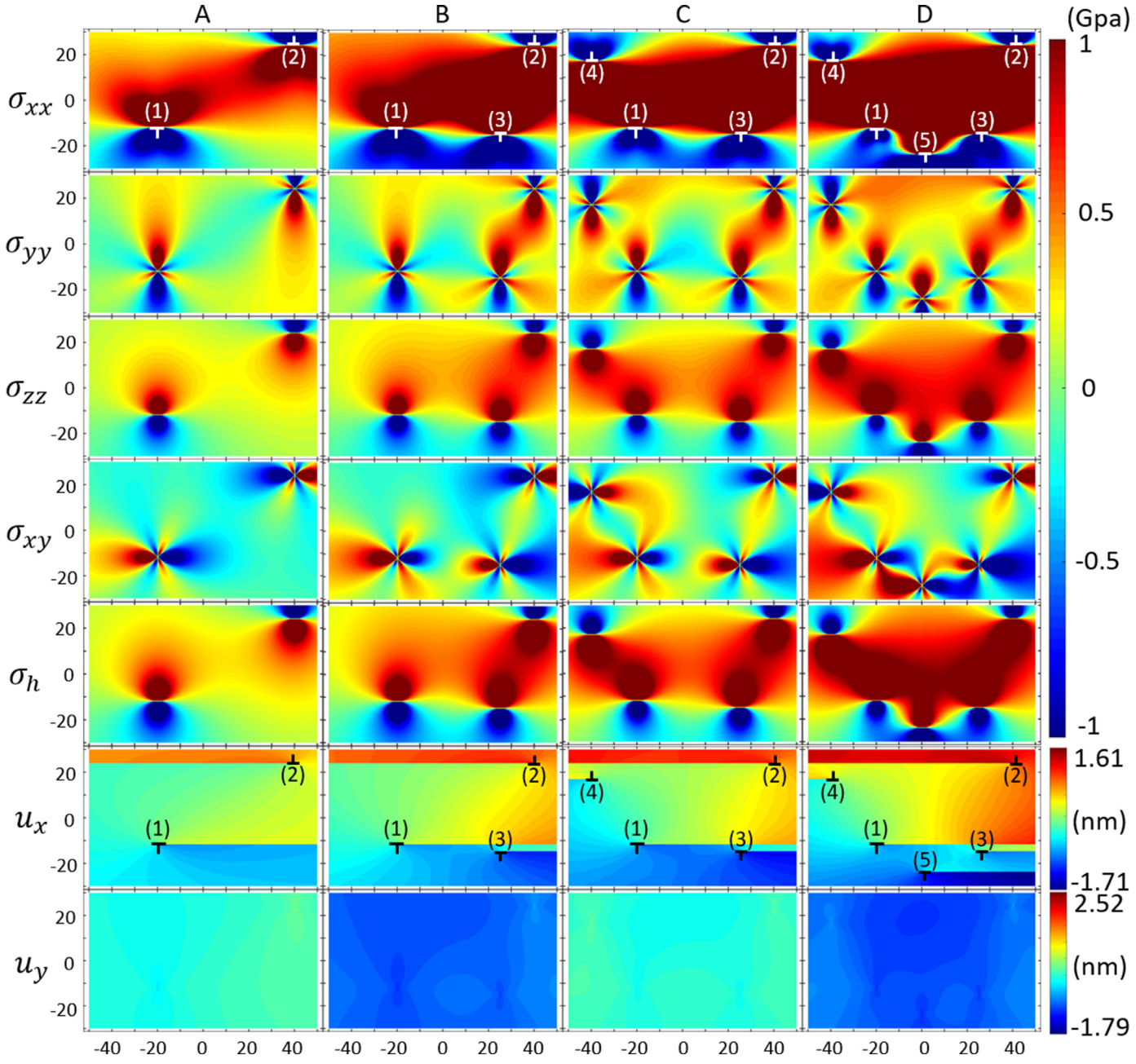

Fig. 3. Stress fields and displacement fields of a Li_YFePO_4 particle for different dislocation densities when dislocation#1 with orientation-3 and phase fraction $x_p = 0.9$. Group A has dislocation#1 and 2. Group B has dislocation#1, 2, and 3. Group C has dislocation#1, 2, 3, and 4. Group D has dislocation#1, 2, 3, 4, and 5. The Burgers vectors of dislocation#1, 2, 3, 4, and 5 are (-1, 0), (1, 0), (-1, 0), (1, 0), and (-1, 0), respectively. With a higher dislocation density, the larger average value of hydrostatic stress $\sigma_h = (\sigma_{xx} + \sigma_{yy} + \sigma_{zz})/3$ suggests a higher electrical potential of the particle. The sharp interfaces in displacement fields indicate where the slip planes of dislocations locate.

tion#1 exhibits the highest electrical potential, and the CV curve with orientation-1 (1, 0) for dislocation#1 shows the weakest shift and distortion. We may hence promote the kinetic performance of Li_YFePO_4 cathode materials by increasing the density and tailoring the orientations of dislocations.

To illustrate the effects of scanning rates, the influences of the density and orientation of dislocations on CV curves are presented in Fig. 5, where the scanning direction and the overpotential range of two-phase coexistence (the gray region) are the same as those in Fig. 4. Both the orientation of dislocation#1 and the dislocation density of the particle influence the peak current density (i.e., the peak value of i) and the peak overpotential (i.e., the value of $\Delta\varphi$ corresponds to the peak current density) of CV curves. For each scan rate v in Fig. 5, the CV curve in group D (i.e., contains the most number of dislocation density) with orientation-3 (-1, 0) displays the highest peak current density and peak overpotential ((Fig. 5**l**). Based on the Randles-Sevcik equation (Eq. (11)), the highest peak current density indicates the highest effective diffusivity, which implies that the effective diffusivity of a Li_YFePO_4 particle may be increased by adjusting the characteristics of dislocations. With a higher scanning rate, dislocations have stronger effects on determining the peak current density and peak overpotential. By comparing the CV curves of group A with orientation-1 (1, 0) (Fig. 5**a**) with the CV curves of group D with orientation-3 (-1, 0) in Fig. 5**l**, we can see that (1) the peak current densities during delithiation increase from 1.267 mA/cm^2 to 2.164 mA/cm^2 (1.708 times) for v = 1 mV/s, and from 7.325 mA/cm^2 to 14.258 mA/cm^2 (1.946 times) for

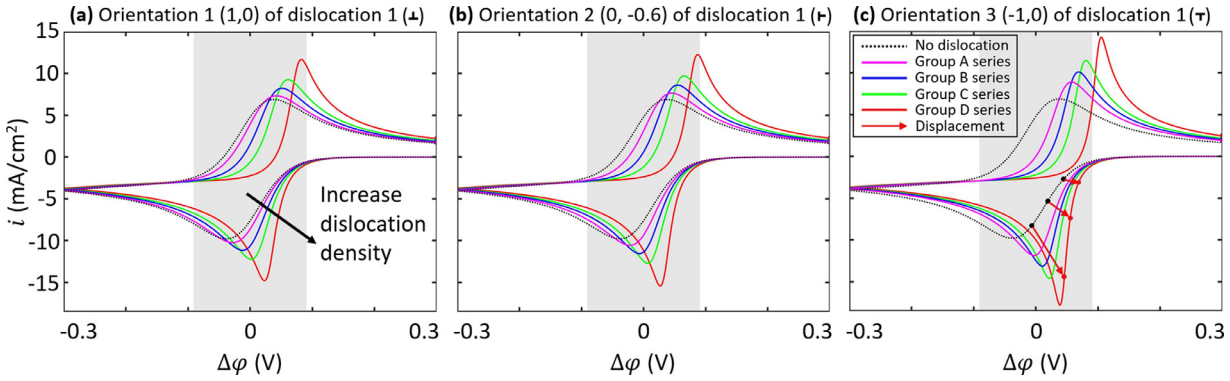

Fig. 4. CV curves for different dislocation densities of a Li_YFePO_4 particle, where dislocation#1 with **(a)** orientation-1 (1, 0), **(b)** orientation-2 (0, -0.6), and **(c)** orientation-3 (-1, 0). The scan rate of every CV curve is 16 mV/s. The gray region indicates the overpotential of two-phase coexistence ($0 < x_p < 1$). From group A to group D, the dislocation density increases. For every orientation of dislocation#1, the CV curve with a higher dislocation density shows a larger displacement relative to the CV curve with no dislocation. The displacement of CV curves consists of shift and distortion, which depend on the density and orientation of dislocations. For each dislocation density, orientation-3 (-1, 0) displays the strongest shift and distortion, and orientation-1 (1, 0) shows the weakest shift and distortion. The kinetic performance of electrodes may hence be promoted by increasing the dislocation density and adjusting the orientations of dislocations.

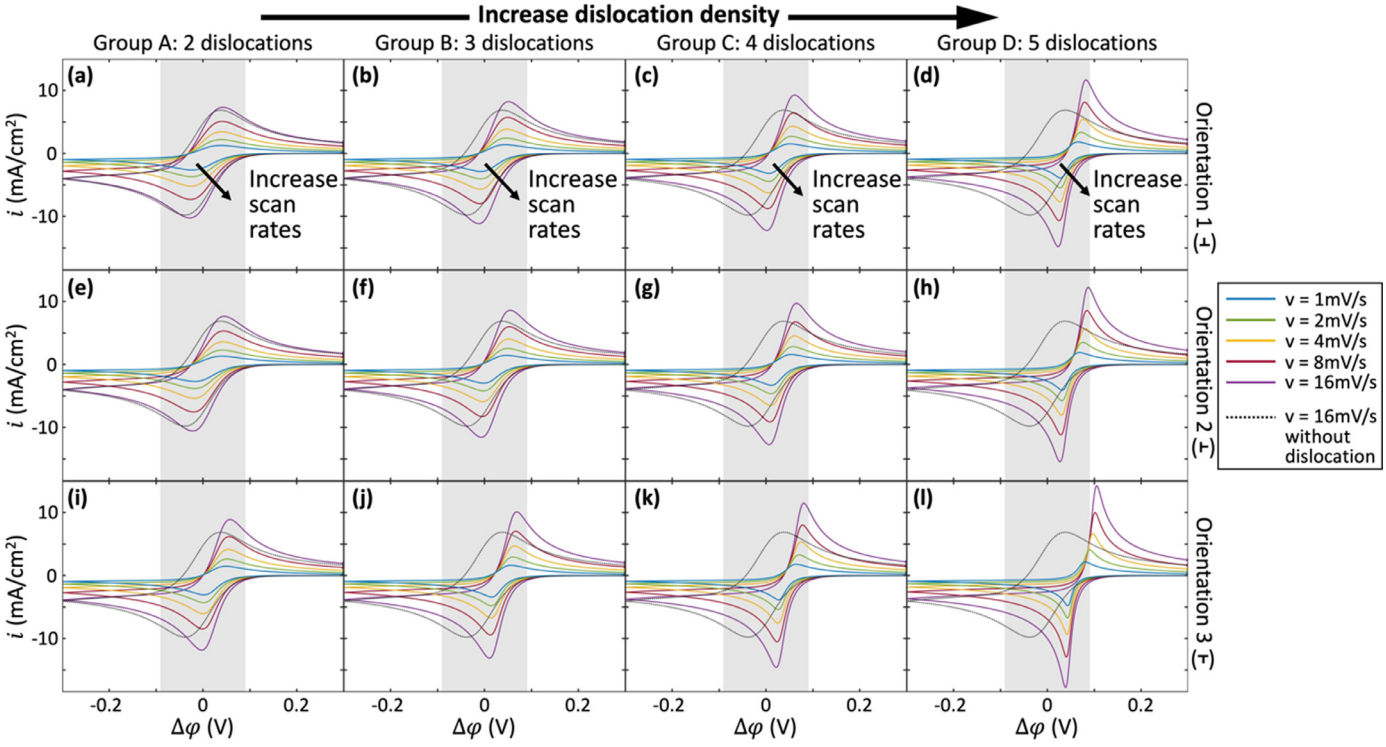

Fig. 5. CV curves of a Li_YFePO_4 particle for different scan rates with different orientations of dislocation#1 and different dislocation densities. The gray region indicates the overpotential of two-phase coexistence ($0 < x_p < 1$). From group A to group D, the dislocation density increases. For every scan rate (v), the peak current density (the peak value of i) and peak overpotential ($\Delta\varphi$ corresponding to the peak current density) of CV curves depend on both the orientation of dislocation#1 and the dislocation density of the particle. The CV curves in group D with orientation-3 (-1, 0) (**Fig. 5l**) display the highest peak current density and peak overpotential for all scan rates, which implies the highest effective diffusivity of Li and the largest electrical power. With a higher scan rate, dislocations have stronger effects on increasing the peak current density and peak overpotential, which suggests that the kinetic performance of the particle with a stronger non-equilibrium state may be promoted more by adjusting dislocations.

$v = 16$ mV/s, and (2) the corresponding peak overpotential increase from 0.038 mV to 0.08 mV (2.105 times) for $v = 1$ mv/s, and from 0.042 mV to 0.106 mV (2.524 times) for $v = 16$ mV/s. This result indicates that the dislocation-promoted electrical power is larger for a higher scanning rate. Because a larger scanning rate represents a stronger non-equilibrium state of the particle, the electrochemical performance of Li_YFePO_4 (dis)charged with a higher C-rate (i.e., under a stronger non-equilibrium state) may be enhanced by the existence of dislocations.

The average value of the hydrostatic stress, σ_{hAVG} in the modified Butler-Volmer equation (Eq. (9)) is the key parameter connecting effects of dislocations and electrochemical performance for a Li_YFePO_4 particle. With the increased dislocation density, the change of the average hydrostatic stress, $\Delta\sigma_{hAVG}$, between different dislocation groups is presented in Fig. 6**a**. $\Delta\sigma_{hAVG}$ is shown to be larger than zero for every dislocation density, indicating the particle is in tension due to dislocations for both Li-rich phase (denote in á) and Li-poor phase (denote in £). The modified Butler-Volmer equation (Eq. (9)) suggests that $\Delta\sigma_{hAVG} > 0$ leads to the increase of electrical potential for the same current density, as shown in Figs. 4 and 5, which also increases electrical power. A varied $\Delta\sigma_{hAVG}$ value in Fig. 6**a** suggests a nonlinear relation be-

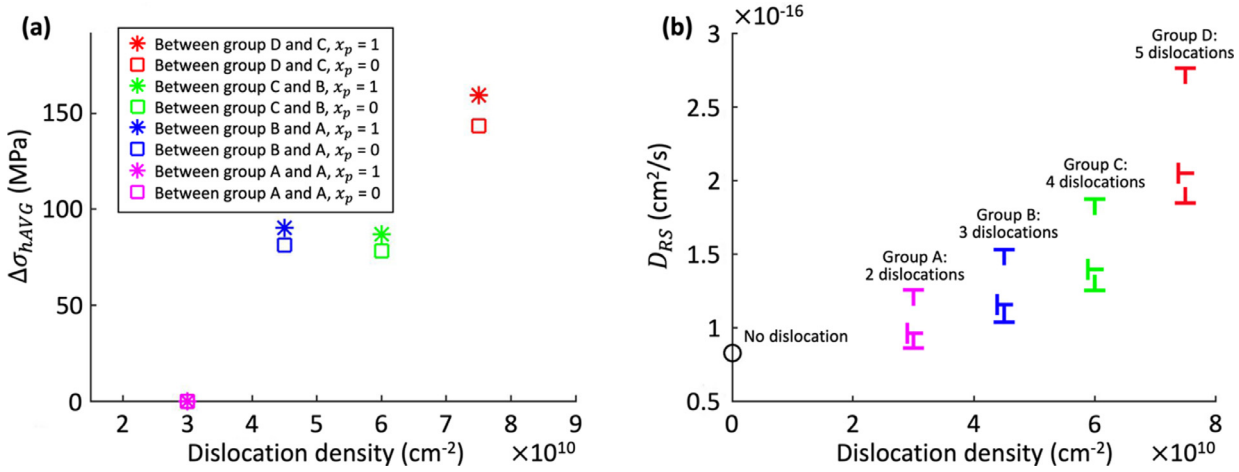

Fig. 6. **(a)** $\Delta\sigma_{hAVG}$, the change of the average hydrostatic stress of a Li_YFePO_4 particle when the dislocation density increases, with phase fraction x_p= 0 and x_p= 1. $\Delta\sigma_{hAVG} > 0$ indicates that dislocations may help Li_YFePO_4 be in tension. The nonconstant $\Delta\sigma_{hAVG}$ shows the nonlinear relation between the stress and dislocation density. The difference of $\Delta\sigma_{hAVG}$ between x_p= 0 and x_p= 1 induced by the phase transformation suggests the different effects of dislocations for different states of charge (SOCs). **(b)** D_{RS}, the effective diffusivities calculated by the Randles-Sevcik equation [43] for different dislocation densities with different orientations of dislocation#1. The particle with a larger dislocation density has a higher D_{RS}, especially for orientation-3 (-1, 0), which implies that increasing the dislocation density and adjusting the dislocation orientation may promote the kinetic performance of the electrodes in lithium-ion batteries.

tween the stress and dislocation density for the particle. By increasing the dislocation density is not sufficient to increase σ_{hAVG}, because $\Delta\sigma_{hAVG}$ is determined by both the location and the orientation of any additional dislocation, which is noticeable by comparing Figs 1–3. Tailoring these characteristics of dislocations is essential for promoting the kinetic performance of a Li_YFePO_4 particle.

Because of the different stiffness coefficients between the Li-rich phase (denote in á) and the Li-poor phase (denote in £), the $\Delta\sigma_{hAVG}$ with $x_p = 1$ is observed higher than the $\Delta\sigma_{hAVG}$ with $x_p = 0$ for every dislocation density in Fig. 6**a**. Based on the modified Butler-Volmer equation (Eq. (9)), the electrical potential of a discharged Li_YFePO_4 particle is hence increased more by the existence of dislocations than that of a charged particle. Therefore, among the particles with the same initial and final electrical potentials during (dis)charging, the particle with dislocations may have larger change of SOC than the particle without dislocations. This mechanism suggests that adding dislocations may help LiFePO4 cathode materials mitigating the capacity loss during (dis)charging. Fig. 6**a** shows that the difference of $\Delta\sigma_{hAVG}$ between $x_p = 1$ and $x_p = 0$ is larger when the $\Delta\sigma_{hAVG}$ of $x_p = 0$ is larger, which suggests that a larger $\Delta\sigma_{hAVG}$ from additional dislocations may increase the capacity. Thus, the increase of capacity could be achieved by carefully adding dislocations.

The dislocation-affected electrochemical performance of a Li_YFePO_4 particle can be reflected by the increased effective diffusivity as shown in Fig. 6**b**. With the peak current densities during lithiation at different scan rates (Fig. 5), the effective diffusivity D_{RS} of Li is calculated using the Randles-Sevcik equation (i.e., Eq. (11)). D_{RS} is a parameter that reveals the combined effects of the bulk diffusivity D of Li in the particle and the rate of the chemical reaction on the particle surface. A larger D_{RS} represents a faster (de)lithiation. Fig. 6**b** shows that D_{RS} is higher for a particle with higher dislocation density; and the increase rate of D_{RS} depends on the orientation of dislocation#1 and the dislocation density of the particle. For group D with orientation-3 (-1, 0), $D_{RS} = 2.72\times10^{-16}$ cm^2/s, which is 3.3 times larger as compared with D_{RS} for no dislocation (0.826×10^{-16} cm^2/s). Hence, we may improve the effective diffusivity of Li_YFePO_4 cathodes by introducing dislocations with increased density and carefully chosen orientation. In the observation of Singer et al. [4], the dislocation density was larger for a higher voltage of the cathode VS Li^+ (a higher SOC). Although what they measured were Li-rich layered oxides, we may expect that the Li_YFePO_4 cathode with a higher SOC has a larger effective diffusivity, once the orientations of dislocations are justified.

Besides the increased density and carefully chosen orientations of dislocations, the variational partial molar volume of Li is also a key factor of the increased effective diffusivity in Fig. 6**b**. This relation can be qualitatively interpreted by following steps: (1) The area under a CV curve between the minimal overpotential $\Delta\varphi_{MIN}$ and the maximal overpotential $\Delta\varphi_{MAX}$ during the 1st half scan is denoted by A, which is determined by the discharged electric charge quantity because of the equality below:

$$A = \int_{\Delta\varphi_{MAX}}^{\Delta\varphi_{MIN}} id\Delta\varphi = \int_{t_1}^{t_2} ivdt = v\int_{t_1}^{t_2} idt = vQ,$$

where t_1 and t_2 are the initial and final time of the 1st half CV scan, respectively; and Q is the discharged electric charge quantity. (2) As discussed above, dislocations may increase the capacity during (dis)charging. For the same scanning rate with the orientation of dislocation#1, the particle has more dislocations may thus be discharged with more electricity during the 1st half scan, suggesting that the absolute value of A for the CV curve should be equal to or larger than that for the CV curve of a particle with lesser dislocations. It is consistent with the CV curves observed in Figs. 4 and 5. (3) The CV curves with dislocations can be considered as being transformed from one with no dislocation. The transformation can be characterized by the displacement of CV curves relative to the one with no dislocation in the coordinate system, which is shown in Fig. 4**c**. The displacement of CV curves consists of a shift and a distortion which indicate rigid movement and shape changes, respectively. (4) The CV curves are generated based on Fick's law (Eq. (7)), whose boundary conditions include the modified Butler-Volmer equation (Eq. (9)). Mathematically, the term $\sigma_{hAVG}\Omega$ in Eq. (9) represents the horizontal shift of CV curves in the CV coordinate system. If $\sigma_{hAVG}\Omega$ is a constant value during scanning, the displacement of CV curves is horizontal and evenly distributed, as shown in Dhiman and Huang [25]. In this case, the CV curves for particles with different characteristics of dislocations should have the same shape at different horizontal locations in the CV coordinate system, and then the corresponding peak cur-

rent densities of CV curves are all the same. (5) For variational Ω expressed by the molar fraction of Li (Eq. (10)), $\sigma_{hAVG}\Omega$ increases with the increased y_{Li} during scanning, suggesting that the distances of the horizontal shift of CV curves are smaller at the beginning of scans when y_{Li}value is small. With a variational horizontal shift, to keep the absolute value of area A for the CV curve equal to or larger than that for the one for particles without dislocations, the CV curve for particles with dislocations would be distorted. In this case, the curves are no longer horizontally shifting with the same distance at different locations in the CV coordinate system. That is, distortion is introduced to compensate the effects of variational $\sigma_{hAVG}\Omega$, as shown in Fig. 4**c**. (6) For a bigger σ_{hAVG} value, $\sigma_{hAVG}\Omega$ has a larger variation, and it indicates a stronger distortion. This result explains that the particle with more dislocations exhibits a larger absolute value of the peak current density in the 1st half CV scan, as shown in Figs. 4 and 5. (7) The peak current density in the 1st half scan is used for calculating the effective diffusivity in the Randles-Sevcik equation (i.e., Eq. (11)). Based on a variational Ω, the particle with a larger σ_{hAVG} value is therefore has a higher effective diffusivity D_{RS} as displayed in Fig. 6**b**.

As shown in Figs. 4 and 5, the CV curves for particles has more dislocations has stronger distortion, which makes the part of the curve of the 1st half scan closer to the part of the curve of the 2nd half scan. Mathematically, there should be intersections in a CV curve if the term $\sigma_{hAVG}\Omega$ in Eq. (9) is large enough. However, for Li_YFePO_4 cathodes, the CV curve with intersections has not been observed yet in experiments. Due to the limited effective diffusivities, it might confine the influence of dislocations on peak current density. Dislocation-induced distortions of CV curves may hence be spontaneously restricted to avoid the intersections, which mitigate dislocation effects.

Compared to the CV curves with the constant partial molar volume shown in Dhiman and Huang [25], the CV curves in this study are distorted due to the variational partial molar volume, as discussed above, suggesting that using carefully tailored dislocations to promote the effective diffusivity of lithium is suitable for the electrodes whose partial molar volumes are functions of the SOC or Li concentration. The variational partial molar volume may also be revealed under nonequilibrium state. Due to the solid viscosity during the nonequilibrium process, the volume change of electrodes may be delayed relative to the fraction change of Li, which has been shown in the experimental study of Liu et al. [45] and modeling study of Chen and Huang [29]. The delay indicates that the effective partial molar volume is variational during (de)lithiation, even if the intrinsic partial molar volume is constant. The increase of the effective diffusivity is more noticeable for the electrode under a stronger non-equilibrium process, as mentioned above. To include the electrochemical polarization in the non-equilibrium process, the extent of two-phase coexistence in CV spectra (the gray zone in Figs. 4 and 5) in this study is wider than that in Dhiman and Huang [25], which makes the stiffness change induced by the phase transformation becoming more gradual. In contrast, the sharper change of stiffness in the narrower extent of two-phase coexistence in Dhiman and Huang [25] leaded to small fluctuations of CV curves in the two-phase coexistence regions (cf. Figs. 4 and 5 in Dhiman and Huang [25]).

The dislocation density and dislocation-induced stress in most existing studies were formulated using the equations below [1]:

$$\rho = \frac{\beta}{b}\frac{\partial c}{\partial r}, \tag{12}$$

$$\sigma_d = M\chi\mu b\sqrt{\rho}, \tag{13}$$

where ρ is the dislocation density, β is lattice contraction coefficient, b is the magnitude of the Burgers vector, $\partial c/\partial r$ is the concentration gradient, σ_d is the dislocation-induced stress, M is the Taylor orientation factor, χ is the empirical constant, and μ is the shear modulus. For example, Ma et al. [46] modeled the composition of ρ for dislocation-induced softening effect and incorporated σ_d in the plastic constitutive model of electrodes [47], which is based on the assumption that dislocations would reduce strain energy (i.e., diffusion-induced stress). With this assumption and the traditional dislocation-induced stress model (i.e., Eqs. (12) and (13)), diffusion-induced stress was simulated to be reduced by σ_d in the electrodes with different geometries (Wei et al. [1], Li et al. [2], Liu et al. [18], Li et al. [19], Zhu et al. [20]), which is different from our study about $\Delta\sigma_{hAVG}$ shown in Fig. 6**a**. This contrary exists because the above assumption is limited for the case of spontaneously generated dislocations, and it is not applicable for pre-existing engineered dislocations investigated in this study. This is the main reason why the dislocations in above articles [1,2,18–20] were named diffusion-induced misfit dislocations. Unlike the spontaneously generated dislocations, the engineered dislocations have the freedom of desired orientation. Therefore the stress induced by engineered dislocations should be described by Eq. (1) instead of Eqs. (12) and (13). Furthermore, Eqs. (12) and (13) are based on continuous dislocation density field and isotropic material property, which is only valid for large electrode particles and polycrystal. In contrast, our study focuses on nano-sized electrode particles. Compared to large electrode particles, a nanoparticle has a lower quantity of dislocations and has a stronger tendency of being single crystal, therefore it should be described by an anisotropic discrete dislocation model (i.e., Eqs. (1) to (6)). The discrete dislocation model in this study reveals the singularity of stress fields at dislocation cores, as shown in Figs. 1–3, which indicate the influences of the distribution and orientation of dislocations. Although a smaller nanoparticle has less dislocations, the effect of the singularity of each dislocation core is relatively stronger on the stress fields. Hence, it is more necessary to consider the discreteness of dislocations for smaller electrode particles.

4. Conclusion

Based on linear elastic mechanics and the superposition principle, we have modeled the stress and displacement field induced by the dislocations with arbitrary distribution and orientations in an electrode particle. The dislocation-induced stress is introduced into the electrochemical reaction on the particle surface using the modified Butler-Volmer equation which is a boundary condition of Fick's law used for governing the diffusion of lithium. The phase-fraction dependent anisotropic stiffness of electrode materials is incorporated in this study. The partial molar volume of lithium is considered as a function of the molar fraction of occupied Li sites during (de)lithiation.

We reported the stress and displacement fields of a Li_YFePO_4 particle model for four groups of dislocations with different dislocation densities. Every group includes a dislocation with a variational dislocation orientation. The CV curves of the particle for all densities and orientations of dislocations under different scanning rates are numerically solved using the finite difference method coded with MATLAB. The peak current densities in the CV curves are utilized into the Randles-Sevcik equation to identify the effective diffusivities of lithium corresponding to different dislocation characteristics. The influences of dislocations on CV curves and the effective diffusivity are compared with that of the electrode particle without dislocations.

Compared to the electrode particle with no dislocations, increasing the dislocation density can add-up the average stress and the average plastic strain of the particle, which leads to higher electrical potential due to the coupling effect between the mechanical stress and the electrochemical reaction. The increased electrical potential indicates the increase of the electrical energy stored

in the particle, which can be magnified by optimizing the dislocation orientation. Increasing the dislocation density makes CV curves shift and distort, especially for a particular dislocation orientation, representing the improvements of electrical power and the effective diffusivity. Electrical power is improved dramatically when the particle is scanned with a higher rate. Thus, justified dislocations may improve the kinetic performance of electrodes, especially when the electrodes are under stronger non-equilibrium states. Based on the difference between the influences of dislocations on the two phases of Li_YFePO_4, we infer that the capacity loss of the electrodes during (dis)charging may be alleviated by dislocations, especially for higher dislocation densities at certain dislocation orientations.

This study has demonstrated the influences of the density and orientation of dislocations on the mechanical and electrochemical response of a Li_YFePO_4 particle, which suggests the strategy of using engineered dislocations to further improve the performance of electrodes for lithium-ion batteries. Our methodology presents an insight to develop dislocation-involved mechanics and electrochemistry for battery systems.

Declaration of Competing Interest

The authors have no conflict of interest to disclose.

Appendix

The auxiliary angles were expressed in the below arctan functions by Indenbom and Lothe [24],

$$\omega = \tan^{-1}\frac{2r_x r_y \lambda \sin\phi}{r_x^2 - \lambda^2 r_y^2}, \tag{A1}$$

$$\eta_x = \tan^{-1}\frac{r_x^2 \sin 2\phi}{\lambda^2 r_y^2 - r_x^2 \cos 2\phi}, \tag{A2}$$

$$\eta_y = \tan^{-1}\frac{r_y^2 \lambda^2 \sin 2\phi}{r_x^2 - \lambda^2 r_y^2 \cos 2\phi}, \tag{A3}$$

and can be transferred to the forms $\omega = \omega(\psi)$, $\eta_x = \eta_x(\psi)$, and $\eta_y = \eta_y(\psi)$, with $\tan\psi = r_x/r_y$. However, the range of arctan functions is $(-\pi/2, \pi/2)$. Hence the spatial distributions of ω, η_x, and η_y calculated using Eqs. (A1), (A2), and (A3) are discontinuous, respectively along the straight lines whose azimuths ψ_ω^*, $\psi_{\eta x}^*$, and $\psi_{\eta y}^*$ satisfy the equalities $(\tan\psi_\omega^*)^2 = 1/\lambda^2$, $(\tan\psi_{\eta x}^*)^2 = \cos 2\phi/\lambda^2$, and $(\tan\psi_{\eta y}^*)^2 = \sec 2\phi/\lambda^2$. The discontinuous auxiliary angles suggest the discontinuity of the displacement at the azimuths ψ_ω^*, $\psi_{\eta x}^*$, and $\psi_{\eta y}^*$, which are not plasible because ψ_ω^*, $\psi_{\eta x}^*$, and $\psi_{\eta y}^*$ are independent of the Burgers vectors of dislocations. To solve this problem, we use differential forms of Eqs. (A1)–(A3). The auxiliary angles can be obtained by numerically solving the equations $[D_\psi]\cdot\omega = \frac{d\omega}{d\psi}$, $[D_\psi]\cdot\eta_x = \frac{d\eta_x}{d\psi}$, and $[D_\psi]\cdot\eta_y = \frac{d\eta_y}{d\psi}$, where $\frac{d\omega}{d\psi}$, $\frac{d\eta_x}{d\psi}$, and $\frac{d\eta_y}{d\psi}$ are the derivatives yielded from the equality $\tan\psi = r_x/r_y$ and Eqs. (A1)–(A3). To conveniently calculate the auxiliary angles for the dislocation with an arbitrary Burgers vector, the independent variable ψ (the azimuth relative to the coordinate frame) is replaced with Ψ, which is the azimuth relative to the Burgers vector, with the range $-\pi < \Psi \le \pi$ and the equality $\Psi = \psi - \psi_B$, where ψ_B is the azimuth of the Burgers vector.

References

[1] P. Wei, et al., Effects of dislocation mechanics on diffusion-induced stresses within a spherical insertion particle electrode, J. Mater. Chem. A 2 (4) (2014) 1128–1136, doi:10.1039/c3ta13925e.

[2] J. Li, Q. Fang, F. Liu, Y. Liu, Analytical modeling of dislocation effect on diffusion induced stress in a cylindrical lithium ion battery electrode, J. Power Sources 272 (2014) 121–127, doi:10.1016/j.jpowsour.2014.07.191.

[3] P. Yan, J. Zheng, M. Gu, J. Xiao, J.G. Zhang, C.M. Wang, Intragranular cracking as a critical barrier for high-voltage usage of layer-structured cathode for lithium-ion batteries, Nat. Commun. 8 (2017) 1–9, doi:10.1038/ncomms14101.

[4] A. Singer, et al., Nucleation of dislocations and their dynamics in layered oxide cathode materials during battery charging, Nat. Energy 3 (8) (2018) 641–647, doi:10.1038/s41560-018-0184-2.

[5] N.A. Sobolev, Defect engineering in implantation technology of silicon light-emitting structures with dislocation-related luminescence, Semiconductors 44 (1) (2010) 1–23, doi:10.1134/S106378261001001X.

[6] N. Shin, M. Chi, J.Y. Howe, M.A. Filler, Rational defect introduction in silicon nanowires, Nano Lett. 13 (5) (2013) 1928–1933, doi:10.1021/nl3042728.

[7] C. Zhou, et al., Defect engineering for high-performance n-Type PbSe thermoelectrics, J. Am. Chem. Soc. 140 (29) (2018) 9282–9290, doi:10.1021/jacs.8b05741.

[8] C. Yan, G. Chen, J. Sun, C. Lv, J. Pei, Edge dislocation surface modification: a new and efficient strategy for realizing outstanding lithium storage performance, Nano Energy 15 (2015) 558–566, doi:10.1016/j.nanoen.2015.05.011.

[9] D. Wang, X. Wu, Z. Wang, L. Chen, Cracking causing cyclic instability of $LiFePO_4$ cathode material, J. Power Sources 140 (1) (2005) 125–128, doi:10.1016/j.jpowsour.2004.06.059.

[10] F. Shi, Z. Song, P.N. Ross, G.A. Somorjai, R.O. Ritchie, K. Komvopoulos, Failure mechanisms of single-crystal silicon electrodes in lithium-ion batteries, Nat. Commun. 7 (May) (2016) 1–8, doi:10.1038/ncomms11886.

[11] J. Vetter, et al., Ageing mechanisms in lithium-ion batteries, J. Power Sources 147 (1–2) (2005) 269–281, doi:10.1016/j.jpowsour.2005.01.006.

[12] Y.T. Cheng, M.W. Verbrugge, Evolution of stress within a spherical insertion electrode particle under potentiostatic and galvanostatic operation, J. Power Sources 190 (2) (2009) 453–460, doi:10.1016/j.jpowsour.2009.01.021.

[13] S. Kim, H. Chen, H.Y.S. Huang, Coupled mechanical and electrochemical analyses of three-dimensional reconstructed $LiFePO_4$ by focused ion beam/scanning electron microscopy in lithium-ion batteries, J. Electrochem. Energy Convers. Storage 16 (1) (2019) 1–7, doi:10.1115/1.4040760.

[14] A.F. Bower, P.R. Guduru, V.A. Sethuraman, A finite strain model of stress, diffusion, plastic flow, and electrochemical reactions in a lithium-ion half-cell, J. Mech. Phys. Solids 59 (4) (2011) 804–828, doi:10.1016/j.jmps.2011.01.003.

[15] D.M. Piper, T.A. Yersak, S.H. Lee, Effect of compressive stress on electrochemical performance of silicon anodes, J. Electrochem. Soc. 160 (1) (2013) A77–A81, doi:10.1149/2.064301jes.

[16] C.V. di Leo, E. Rejovitzky, L. Anand, Diffusion-deformation theory for amorphous silicon anodes: The role of plastic deformation on electrochemical performance, Int. J. Solids Struct. 67–68 (2015) 283–296, doi:10.1016/j.ijsolstr.2015.04.028.

[17] J. Wen, Y. Wei, Y.T. Cheng, Stress evolution in elastic-plastic electrodes during electrochemical processes: a numerical method and its applications, J. Mech. Phys. Solids 116 (2018) 403–415, doi:10.1016/j.jmps.2018.04.006.

[18] Z. Liu, J. Zhou, B. Chen, J. Zhu, Interaction between dislocation mechanics on diffusion induced stress and electrochemical reaction in a spherical lithium ion battery electrode, RSC Adv. 5 (91) (2015) 74835–74843, doi:10.1039/c5ra13991k.

[19] J. Li, D. Lu, Q. Fang, Y. Liu, P. Wen, Cooperative surface effect and dislocation effect in lithium ion battery electrode, Solid State Ion. 274 (2015) 46–54, doi:10.1016/j.ssi.2015.03.004.

[20] J. Zhu, J. Zhou, B. Chen, Z. Liu, T. Liu, Dislocation effect on diffusion-induced stress for lithiation in hollow spherical electrode, J. Solid State Electrochem. 20 (1) (2016) 37–46, doi:10.1007/s10008-015-2999-0.

[21] T. Maxisch, G. Ceder, Elastic properties of olivine Lix FePO4 from first principles, Phys. Rev. B Condens. Matter Mater. Phys. 73 (17) (2006) 1–4, doi:10.1103/PhysRevB.73.174112.

[22] M.S. Whittingham, Lithium batteries and cathode materials, Chem. Rev. 104 (10) (2004) 4271–4301, doi:10.1021/cr020731c.

[23] H.Y. Shadow Huang, Y.X. Wang, Dislocation based stress developments in lithium-ion batteries, J. Electrochem. Soc. 159 (6) (2012) A815–A821, doi:10.1149/2.090206jes.

[24] V.L. Indenbom, J. Lothe, Elastic Strain Fields and Dislocation Mobility, Volume 31, 1st ed., North-Holland, 1992.

[25] P. Dhiman, H.Y.S. Huang, Dislocation based stresses during electrochemical cycling and phase transformation in lithium-ion batteries, Comput. Mater. Sci. 171 (2019) (2020) 109275 July, doi:10.1016/j.commatsci.2019.109275.

[26] B. Lu, Y. Song, Q. Zhang, J. Pan, Y.T. Cheng, J. Zhang, Voltage hysteresis of lithium ion batteries caused by mechanical stress, Phys. Chem. Chem. Phys. 18 (6) (2016) 4721–4727, doi:10.1039/c5cp06179b.

[27] X. Li, Q. Fang, H. Wu, J. Li, Y. Liu, P. Wen, Misfit dislocations induced by lithium-ion diffusion in a thin film anode, J. Solid State Electrochem. 21 (2) (2017) 419–427, doi:10.1007/s10008-016-3377-2.

[28] U. Ulvestad, et al., Topological defect dynamics in operando battery nanoparticles, Science 348 (6241) (2015) 1344–1347 (1979), doi:10.1126/science.aaa1313.

[29] H. Chen, H.Y.S. Huang, Modeling and simulation of the non-equilibrium process for a continuous solid solution system in lithium-ion batteries, Int. J. Solids Struct. 212 (2021) 124–142, doi:10.1016/j.ijsolstr.2020.11.014.

[30] G. Bucci, Y.M. Chiang, W.C. Carter, Formulation of the coupled electrochemical-mechanical boundary-value problem, with applications to transport of multiple charged species, Acta Mater. 104 (2016) 33–51, doi:10.1016/j.actamat.2015.11.030.

[31] C.V. di Leo, E. Rejovitzky, L. Anand, A Cahn-Hilliard-type phase-field theory for species diffusion coupled with large elastic deformations: Application to

phase-separating Li-ion electrode materials, J. Mech. Phys. Solids 70 (1) (2014) 1–29, doi:10.1016/j.jmps.2014.05.001.
[32] Z. Cui, F. Gao, J. Qu, A finite deformation stress-dependent chemical potential and its applications to lithium ion batteries, J. Mech. Phys. Solids 60 (7) (2012) 1280–1295, doi:10.1016/j.jmps.2012.03.008.
[33] A. Yamada, H. Koizumi, N. Sonoyama, R. Kanno, Phase change in $LixFePO_4$, Electrochem. Solid State Lett. 8 (8) (2005) 409–413, doi:10.1149/1.1945373.
[34] S. Kim, H.Y.S. Huang, Mechanical stresses at the cathode-electrolyte interface in lithium-ion batteries, J. Mater. Res. 31 (22) (2016) 3506–3512, doi:10.1557/jmr.2016.373.
[35] C.K. ChiuHuang, H.Y.S. Huang, Critical lithiation for C-rate dependent mechanical stresses in $LiFePO_4$, J. Solid State Electrochem. 19 (8) (2015) 2245–2253, doi:10.1007/s10008-015-2836-5.
[36] C.K. ChiuHuang, H.Y. Shadow Huang, Stress evolution on the phase boundary in $LiFePO_4$ particles, J. Electrochem. Soc. 160 (11) (2013) A2184–A2188, doi:10.1149/2.079311jes.
[37] R.W. Hertzberg, R.P. Vinci, J.L. Hertzberg, Deformation and Fracture Mechanics of Engineering Materials, 5th Ed., Wiley, 2012.
[38] M. Tang, H.Y. Huang, N. Meethong, Y.H. Kao, W.C. Carter, Y.M. Chiang, Model for the particle size, overpotential, and strain dependence of phase transition pathways in storage electrodes: application to nanoscale olivines, Chem. Mater. 21 (8) (2009) 1557–1571, doi:10.1021/cm803172s.
[39] M. Stern, Closure to 'discussion of "electrochemical polarization, 1. A theoretical analysis of the shape of polarization curves" [M. Stern and A. L. Geary (pp. 56–63, Vol. 104)],'", J. Electrochem. Soc. 104 (12) (1957) 751, doi:10.1149/1.2428473.
[40] H. Wang, et al., Design and synthesis of high performance $LiFePO_4$/C nanomaterials for lithium ion batteries assisted by a facile H+/Li+ ion exchange reaction, J. Mater. Chem. A 3 (15) (2015) 8062–8069, doi:10.1039/c5ta00178a.
[41] J.P. Jegal, K.B. Kim, Carbon nanotube-embedding LiFePO4 as a cathode material for high rate lithium ion batteries, J. Power Sources 243 (2013) 859–864, doi:10.1016/j.jpowsour.2013.06.090.
[42] P. Zanello, Inorganic Electrochemistry: Theory, Practice, and Application, Royal Society of Chemistry, 2003.
[43] A.J. Bard, L.R. Faulkner, Electrochemical Methods: Fundamentals and Applications, 2nd ed., Wiley, 2000.
[44] A. Yamada, et al., Room-temperature miscibility gap in LixFePO4, Nat. Mater. 5 (5) (2006) 357–360, doi:10.1038/nmat1634.
[45] H. Liu, et al., Capturing metastable structures during high-rate cycling of $LiFePO_4$ nanoparticle electrodes, Science 344 (6191) (2014) 1252817 (1979), doi:10.1126/science.1252817.
[46] Z. Ma, Z. Xie, Y. Wang, C. Lu, Softening by electrochemical reaction-induced dislocations in lithium-ion batteries, Scr. Mater. 127 (2017) 33–36 Jan., doi:10.1016/j.scriptamat.2016.08.032.
[47] Z. Ma, H. Wu, Y. Wang, Y. Pan, C. Lu, An electrochemical-irradiated plasticity model for metallic electrodes in lithium-ion batteries, Int. J. Plast. 88 (2017) 188–203 Jan., doi:10.1016/j.ijplas.2016.10.009.
[48] A.V. Churikov, A.V. Ivanishchev, I.A. Ivanishcheva, V.O. Sycheva, N.R. Khasanova, E.V. Antipov, Determination of lithium diffusion coefficient in LiFePO4 electrode by galvanostatic and potentiostatic intermittent titration techniques, Electrochim. Acta 55 (8) (2010) 2939–2950, doi:10.1016/j.electacta.2009.12.079.